Research Article

Check for updates

Geo-environmental properties and microstructural characteristics of sustainable limestone calcined clay cement (LC3) binder treated Zn-contaminated soils

Haoliang WU[1,2✉], Heng SONG[3], Xinpo SUN[3], Yuzhang BI[4], Shenjing FU[3], Ning YANG[3]

[1]*Guangdong Key Laboratory of Marine Civil Engineering, School of Civil Engineering, Sun Yat-sen University, Guangzhou 510275, China*
[2]*Southern Marine Science and Engineering Guangdong Laboratory (Zhuhai), Zhuhai 519082, China*
[3]*College of Civil Engineering, Sichuan University of Science & Engineering, Zigong 643002, China*
[4]*School of Transportation, Southeast University, Nanjing 210096, China*

Abstract: Limestone calcined clay cement (LC3) is an environment-friendly and sustainable cementitious material. It has recently gained considerable attention for the stabilization/solidification (S/S) of soils contaminated by heavy metals. However, the existing studies on S/S of Zn-contaminated soils using LC3 in terms of hydraulic conductivity and microstructural properties as compared to ordinary Portland cement (OPC) are limited. This study focuses on the evaluation of the mechanical, leaching, and microstructural characteristics of Zn-contaminated soils treated with different contents (0%, 4%, 6%, 8%, and 10%) of low-carbon LC3. The engineering performance of the treated Zn-contaminated soils is assessed over time using unconfined compressive strength (UCS), hydraulic conductivity (k), toxicity characteristic leaching procedure (TCLP), and synthetic precipitation leaching procedure (SPLP) tests. Experimental results show that the UCS of Zn-contaminated soils treated with LC3 ranged from 1.47 to 2.49 MPa, which is higher than 1.63%–13.07% for those treated with OPC. The k of Zn-contaminated soils treated with LC3 ranged from 1.16×10^{-8} to 5.18×10^{-8} cm/s as compared to the OPC treated samples. For the leaching properties, the leached Zn from TCLP and SPLP is 1.58–321.10 mg/L and 0.52–284.65 mg/L as the LC3 contents ranged from 4% to 10%. Further, the corresponding pH modeling results indicate that LC3 promotes a relatively suitable dynamic equilibrium condition to immobilize the higher-level Zn contamination. In addition, microscopic analyses demonstrate that the formations of hydration products, i.e., $Zn(OH)_2$, Zn_2SiO_4, calcium silicate hydrate (C–S–H), calcium silicate aluminate hydrate (C–A–S–H) gel, ettringite, and $CaZn(SiO_4)(H_2O)$, are the primary mechanisms for the immobilization of Zn. This study also provides an empirical formula between the UCS and k to support the application of LC3-solidified Zn-contaminated soils in practical engineering in the field.

Key words: Limestone calcined clay cement (LC3); Stabilization/solidification (S/S); Zn-contaminated soils; Microstructural characteristics

1 Introduction

As industrialization and urbanization accelerate, soil pollution by heavy metals increases in prominence and poses a significant threat to ecological and environmental security and human health (Chen et al., 2002). Heavy-metal pollution changes the soil structure, properties, and functions and passes through the

✉ Haoliang WU, wuhliang5@mail.sysu.edu.cn

 Haoliang WU, https://orcid.org/0000-0002-2580-6719

food chain to microorganisms and plants, causing health problems for humans (Capasso et al., 2019). Heavy-metal pollution in the soil is a global problem, especially in developing countries, such as China and India (Han et al., 2020). The remediation technology for contaminated soils has attracted engineers' and scholars' attention worldwide. Since heavy-metal pollution is a severe type of pollution that is long-lasting, highly toxic, and easily migrating, the soil that has been contaminated is unable to decompose completely and is difficult to manage (Khalid et al., 2017). In addition, heavy metals alter the soil's physical and chemical properties, leading to complex mechanical properties of geotechnical engineering (Moghal et al.,

2020). Therefore, it is imperative to investigate the appropriate remediation method to meet the engineering requirements.

According to the report of national general survey on soil contamination, the over-standard rates of Zn pollutants are 0.9% (MEP, 2014). The major type of Zn in contaminated soils is preserved as free ions (Zn^{2+}), zinc carbonate ($ZnCO_3$), zinc sulfate ($ZnSO_4$), and zinc sulfide (ZnS) (Paria and Yuet, 2006). In terms of the available remediation techniques, stabilization/ solidification (S/S) is considered as the most suitable for heavy-metal-contaminated soils due to its wide range of engineering applicability (Du et al., 2014; Wu et al., 2018; Pantazopoulou et al., 2020). Furthermore, S/S is, according to USEPA (1992), the best demonstration technology for treating soils contaminated with heavy metals (i.e., Zn, Pb, Cu, Ni) (Liu et al., 2018). Conventionally, ordinary Portland cement (OPC) is the most widely used binder to treat heavy-metal-contaminated soils (Chen et al., 2019; Senneca et al., 2020). However, there are disadvantages associated with OPC binders (i.e., energy consumption and high carbon dioxide emission), limiting the S/S applications in civil engineering scenarios. A method for overcoming this drawback is to incorporate supplementary cementitious materials (SCMs) (i.e., fly ash (FA), ground granulated blast-furnace slag (GGBS), limestone (LS), and metakaolin) (Yadav et al., 2020; Snehal and Das, 2022). The use of SCMs to reduce the amount of cement will become a trend in green materials due to their lower energy consumption and carbon dioxide emission (Choi and Park, 2020).

Wang et al. (2018) developed a novel green remediation method for contaminated sediments using industrial by-products S/S. They found that the addition of Class-F FA and GGBS facilitated the development of compressive strength and effectively immobilized the contaminants in the sediment. Combining nano-$CaCO_3$ with high-volume slag (HVS) and high-volume slag-fly ash concrete (HVS-FA), Hosan and Shaikh (2021) found that the carbon footprint was reduced by 54%. Wang et al. (2021) replaced slag cement with limestone-calcined clay and found that the replacements of 20% and 30% limestone-calcined clay resulted in similar compressive strengths at 28 d and 90 d. By using low-cost and eco-friendly sorbents (i.e., eggshell, banana peels, and watermelon rind), Elbltagy et al. (2021) removed toxic heavy metals from industrial contaminated wastewater. The results revealed that the addition of eggshells increased the removal percentage for all the metals studied. Parus and Framski (2018) used out-of-date coffee as an effective bio-sorbent to remove impurities (i.e., heavy metals) from water. Kua et al. (2016) evaluated the possibility of combining waste coffee grounds (CG) with industrial wastes (i.e., GGBS and FA) into sustainable roadbed construction materials. They found that unconfined compressive strength (UCS) with different proportions of geopolymer materials ranging from 500–1800 kPa, comfortably met the Thailand Highway Department's minimum requirements for subgrade materials (294.2 kPa).

Limestone calcined clay cement (LC3) is a new low-carbon alternative to the conventional OPC binder, and is expected to reduce carbon dioxide emission by ~40%. A significant amount of the clinker in cement is replaced by LS and calcined clay (CC) during the manufacturing process (Scrivener, 2014). It is noted that kaolin clay is readily available in many developing countries (Deng and Shi, 2015). For the production of LC3, the low-calcined grade kaolin clay (~700 °C for kaolin clay vs. ~1300 °C for clinker) generates an activated metakaolin (MK). In the LC3 binder, the MK reacts with calcium hydroxide (CH) and water. It forms calcium silicate hydrate (C–S–H), calcium silicate aluminate hydrate (C–A–S–H), and calcium aluminate hydrate (C–A–H). Additionally, LS can improve the mechanical properties and durability. Further, LS reacts with the aluminum source provided by CH and CC to form monocarbon aluminates. Based on previous research of solidification and stabilization mechanisms (Bucher et al., 2017; Bakera and Alexander, 2019; Tang et al., 2019; Drissi et al., 2021), the hydration products (i.e., C–S–H, C–A–S–H, and C–A–H) in LC3 have the potential to reduce the mobility of heavy metals in the soil matrix. However, the compounds formed by the combination of hydration products and heavy metals may influence the availability of the metal ions for plants. This may cause the further growth and development of plants, which was confirmed in previous studies (Parus and Framski, 2018; Parus et al., 2021).

The LC3 binder stabilized Zn-contaminated soils have been studied by Reddy et al. (2019). Previous investigation showed that LC3 could significantly improve the immobilization of Zn. The formations of tri-calcium silicate ($3CaO \cdot SiO_2$), portlandite ($Ca(OH)_2$), ettringite ($3CaO \cdot Al_2O_3 \cdot 3CaSO_4 \cdot 32H_2O$), and wulfingite ($Zn(OH)_2$)

were mainly S/S mechanisms for Zn-contaminated soils treated by the LC3 binder (Reddy et al., 2019). Further, it is also a high effective method for dealing with soils contaminated by other metals (i.e., Pb and Cd) using LC3 binder (Reddy et al., 2022). Nevertheless, the mechanical properties, leaching performance, and micro-analysis between the conventional OPC and LC3 for solidification of Zn-contaminated soils have not been determined. Previous researchers also noticed that the release rate of pollutants into the environment highly depends on pH (Gu et al., 2020). The purpose of this research is to fill the gap in understanding pH effects on the Zn-contaminants and evaluating the optimal LC3 binder content.

This study aims to investigate the engineering properties and micro-mechanism for effective S/S treatment of contaminated soils using sustainable LC3 as compared to the conventional OPC binder. The UCS, hydraulic conductivity, pH, electrical conductivity (EC), and moisture content were studied to reveal the engineering properties of LC3 and OPC-stabilized Zn-contaminated soils. Further, toxicity characteristic leaching procedure (TCLP) and synthetic precipitation leaching procedure (SPLP) have been conducted for analyzing the leaching performance. Finally, the micro-mechanism has been analyzed and interpreted through the results of X-ray diffraction (XRD) and scanning electron microscope (SEM) with energy dispersive spectrometer (EDS). The results provide a theoretical basis and technical support for the remediation of heavy-metal contaminated clay by S/S treatment technology with a sustainable LC3 binder.

2 Materials and methods

2.1 Raw materials

The natural soil used in this study was collected from a construction site in Zigong, China. Before applying artificial contamination, the particle-size distribution of natural soil was determined using the NKT6100-D laser particle-size analyzer, as shown in Fig. 1. The basic physical and chemical properties of the soil material were determined as shown in Table 1. Commercial #42.5 OPC was obtained from Weifang, China. The calcined kaolin (MK) and LS were provided from a calcining plant in Liaoning Province, China. The main physical properties and chemical components of natural

soil, OPC, MK, and LS were determined by X-ray fluorescence analysis (XRF), as shown in Table 2. The LC3 is composed of 55% OPC, 30% MK, and 15% LS (Avet et al., 2016).
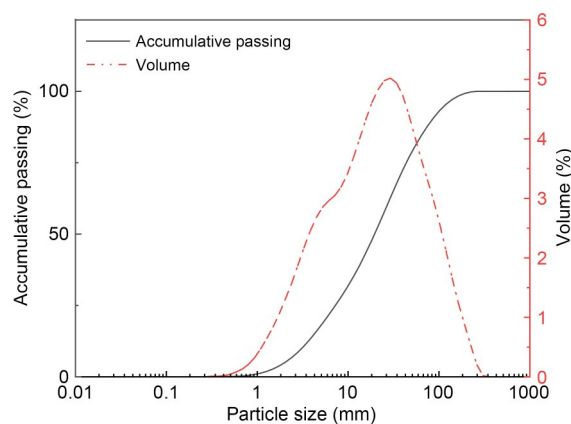

Fig. 1 Particle-size distribution of natural soil

Table 1 Physicochemical properties of natural soil

Parameter	Value
Plastic limit, w_P (%)	18.10
Liquid limit, w_L (%)	29.05
Plasticity index, I_P	10.95
Soil pH	5.87
Natural water content (%)	19.78
Optimal water content, w_{opt} (%)	20.00
Maximum dry density, ρ_d (g/cm^3)	1.70

Table 2 Chemical composition of the raw materials

Component	Mass fraction (%)			
	OPC	CC	LS	Clean soil
SiO_2	24.03	49.97	0.17	22.24
Al_2O_3	8.08	44.53	–	10.04
Fe_2O_3	3.22	2.19	1.03	51.78
CaO	53.04	0.37	98.05	3.21
TiO_2	0.73	2.27	–	2.01
P_2O_5	0.15	0.08	0.39	1.37
MnO	0.15	–	0.06	0.38
MgO	4.84	0.14	0.26	0.32
SO_3	4.12	0.05	–	0.06
K_2O	0.92	0.23	0.04	8.58
Na_2O	0.52	0.06	–	–
Loss on ignition	2.71	1.19	0.35	–

2.2 Sample preparation

Experiments were carried out by using three levels of artificially Zn-contaminated spiked samples,

at 5000 mg/kg (Zn0.5), 10000 mg/kg (Zn1.0), and 15000 mg/kg (Zn1.5), respectively. According to previous research, the soluble nitrate (NO^{3-}) has a tiny influence on the hydration reaction of the S/S binder (Cuisinier et al., 2011). $Zn(NO_3)_2 \cdot 6H_2O$ (analytical grade) was mixed with deionized water to prepare the Zn-contaminated solution. The prepared natural soil was homogeneously mixed with the Zn-contaminated solution and then stored in a container at $T=(20\pm2)$ °C and relative humidity $R_H \geq 95\%$ for 14 d. The aged soil was then oven-dried at 105 °C for 24 h and then manually crushed until passed through a 10-mm sieve. Similar preparation methods have been reported by Du et al. (2014) and Reddy et al. (2019).

The preparation process of LC3 and OPC S/S Zn-contaminated soils is shown in Fig. 2. Firstly, the LC3 content was set to 0% (referred to clean soil), 4%, 6%, 8%, and 10% based on the dry weight of the soil solid, respectively. The 6%- and 8%-OPC binders were prepared for the comparison groups. Secondly, the moisture content was set at approximately 20% reaching its optimal water content with pouring deionized water. An electronic stirrer was used to mix it for 6 min to achieve uniformity fully. Finally, the mixture was compacted into a 40 mm×40 mm×40 mm cubic mold and a 50 mm×50 mm×100 mm cylindrical mold with a hydraulic jack to ensure the dry density reached approximately 1.70 g/cm³. The results of all tests in this study are averaged over three duplicates. After curing at 60 °C for 24 h, the samples were carefully squeezed out of the mold and sealed in a black polyethylene bag for standard curing ($T=22$ °C and $R_H=95\%$) for 7, 14, and 28 d, separately.

2.3 Test methods

2.3.1 Unconfined compressive strength

The UCS test was conducted with a microcomputer-controlled testing machine YSD-2A after curing the samples for 7, 14, and 28 d. A 1-%/min strain rate was performed on all stabilized and untreated samples. The pH, EC, moisture content, and dry density of all broken samples were measured after the UCS test. The soil pH value was obtained from the solid-liquid ratio of 1:1. Moisture content and dry density were determined by heating the soil in an oven with a temperature of 105 °C for 24 h according to MWR (2019).

2.3.2 Hydraulic conductivity

Before the hydraulic conductivity test, all curing 28-d samples were saturated for 24 h. The confining pressure and osmotic pressure were 400 and 300 kPa, respectively. The calculation formula for hydraulic conductivity is:

$$k = \frac{\Delta Q L}{A P \Delta t}, \qquad (1)$$

where k is the hydraulic conductivity (cm/s); ΔQ represents the penetration volume (mL) within time interval Δt; L is the sample height (cm); A is the cross-section area (cm²) of the sample; P is the osmotic
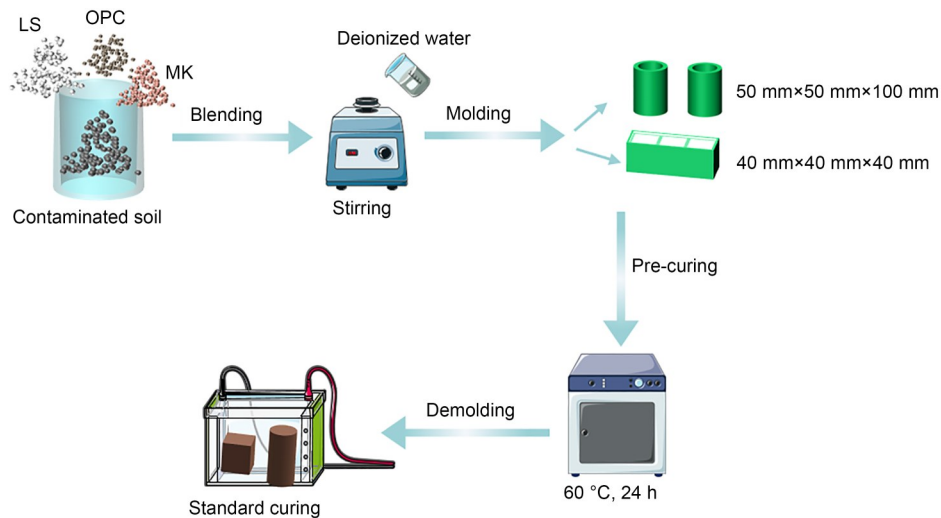

Fig. 2 Schematic illustration for the preparation of LC3 and OPC S/S Zn-contaminated soil samples

pressure (kPa); Δt represents the penetration time interval (s).

2.3.3 TCLP and SPLP tests

The TCLP and SPLP tests were performed following USEPA methods 1311 and 1312 (USEPA, 1992, 1994), respectively. The TCLP and SPLP extractions were prepared with sodium acetate buffer solution of pH=4.93±0.05 and HNO_3-H_2SO_4 solution of pH=4.20±0.05, respectively. A certain weight of the crushed dried sample after the UCS test was ground to pass through a 2-mm sieve. The mass ratio of soil powder and the prepared extraction solution mixed was 1:20 in a 1-L plastic container. The plastic containers were then placed on the tumbler and the mixture was shaken at 30 r/min for (18±2) h. The concentration of Zn ions released from the solution was determined using inductively coupled plasma-optical emission spectrometer (ICP-OES). Then the pH of the electrolyte was measured and recorded with the METTLER TOLEDO-SG23 multiparameter tester.

2.3.4 Chemical equilibrium model

The chemical equilibrium model of S/S Zn-contaminated soils was analyzed by Visual MINTEQ 3.1. The input parameters were obtained from the XRF (Table 2). The total Zn concentration and pH-dependent curve were calculated using thermodynamic data and equilibrium constants from the Visual MINTEQ database, which relies on the National Institute of Standards and Technology (NIST) critical stability constant database (database NIST 46.7).

2.3.5 Microstructure characterization

Some samples from the crushed UCS specimens were ground and passed through 0.075-mm sieves. Approximately 2 g of LC3 and OPC treated samples were removed and air-dried for XRD testing. XRD tests were performed on an X'Pert Pro MPD using a Cu-Kα source at a wavelength of 0.15405 nm. The instrument operates at 40 kV and 20 mA. The step size used is 2θ=0.02°, and the scanning speed is 5 s/step. Samples were analyzed over a 2θ range of 5° to 70°. A subsample of about 1 cm^3 was taken from the broken UCS sample and carefully preserved. The sample was then rapidly frozen in liquid nitrogen at −195 °C, and then held under vacuum at −80 °C for 24 h until the sample was completely lyophilized. The samples were then analyzed by SEM using a 5-kV accelerating high-resolution voltage device TM3030.

3 Results and analysis

3.1 Unconfined compressive strength

The variation of average UCS with LC3 content and Zn concentration at different curing times from 7 to 28 d is presented in Fig. 3. As expected, the increases of the LC3 content and curing ages lead to a significant increment of compressive strength, which is attributed to the formation of hydration products. For instance, with a Zn concentration of Zn0.5, the UCSs of 4%-LC3 and 10%-LC3 samples reach 1.79 and 2.49 MPa after curing for 28 d. These are much higher than the UCS of untreated contaminated samples (UT). For the samples with the same LC3 content and curing conditions, an increased Zn-concentration level results in a decrease in the UCS. It can be seen that the UCSs of 4%-LC3 and 10%-LC3 samples decreased by 0.17 and 0.47 MPa in 28 d, respectively, as compared to the contaminated Zn increasing from Zn0.5 to Zn1.5.

3.2 Hydraulic conductivity

The hydraulic conductivity k of Zn-contaminated soils treated by LC3 and OPC binder at 28-d curing age is shown in Fig. 4. k increases with the increase of Zn concentration regardless of the LC3 and OPC binders. For example, k increases by 1.14–2.17 times as the concentration of Zn added at a concentration ranging from Zn0.5 to Zn1.5 (i.e., 1.16×10^{-8}–3.93×10^{-7} cm/s for Zn0.5 vs. 2.53×10^{-8}–5.89×10^{-7} for Zn1.5). The inhibition of the hydration reaction by Zn is mainly attributed to the generation of Zn_2SiO_4 (Section 3.4). Additionally, k decreases with the increase of the LC3 content under the same conditions of Zn concentration (i.e., 4.44×10^{-8} cm/s for 4% LC3 vs. 2.23×10^{-8} cm/s for 10% LC3 at Zn1.0). It also could be seen that k for Zn-contaminated soils treated by LC3 is lower than that for the OPC binder (i.e., 2.36×10^{-8}–4.76×10^{-8} cm/s for the 6%–8% LC3 vs. 2.99×10^{-8}–5.89×10^{-8} for the 6%–8% OPC).

By using the slope method, it is possible to determine the impact of Zn concentration and binder content on k. From the slope results as plotted in Fig. 4, a significant reduction of k is observed as binder content
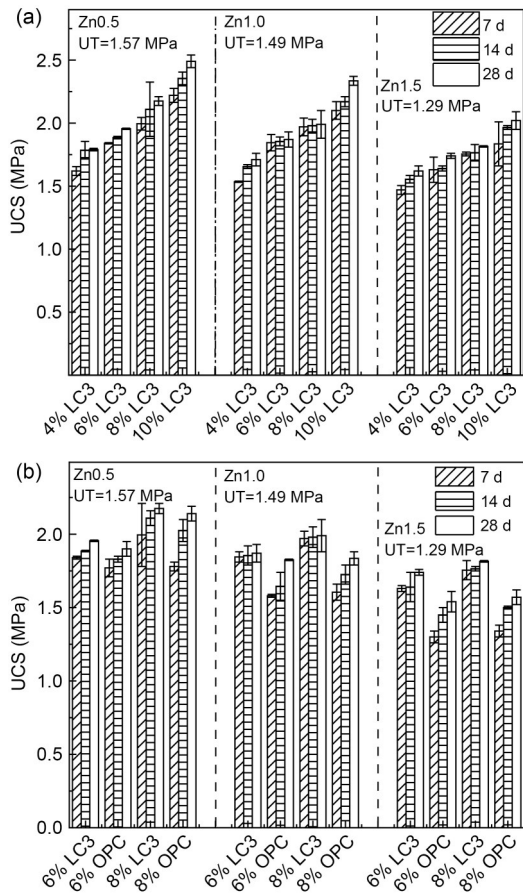
Fig. 3 Variation of UCS at different Zn concentrations and curing ages: (a) LC3 content; (b) LC3 vs. OPC
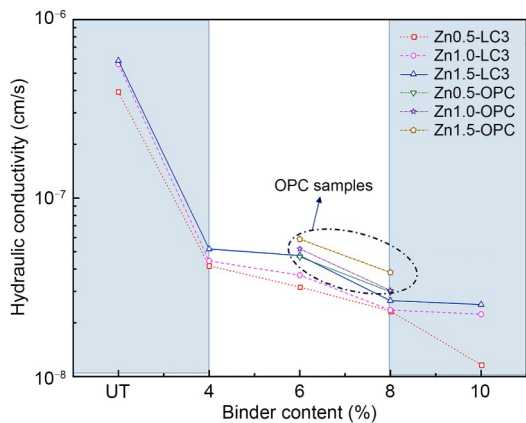

Fig. 4 Hydraulic conductivity of Zn-contaminated soils treated by LC3 and OPC at curing 28 d. References to color refer to the online version of this figure

is increased to 4%. In comparison, the reduction tendency gradually decreases with the increasing binder ratio from 4% to 8%. It can also be noted that the reduction in k becomes very slight as the binder content

is greater than 8%. In addition, the increased Zn concentration has a relatively slight effect on the variation of k regardless of the binder content. From the aspect of reducing the k value, it can be concluded that the optimal dosage of LC3 for the treatment of high-concentration Zn-contaminated soils is 4%–8%.

3.3 TCLP and SPLP

The concentration of leached Zn and pH of LC3 stabilized soils in the TCLP test after curing for 28 d are presented in Fig. 5a. The leached Zn concentration of untreated samples is much higher than the regulatory limit (100 mg/L in (SEPA, 2007)), whereas the leached Zn of treated samples is lower than the criterion except for the 4% LC3 with Zn1.5. It can be seen that the leached Zn decreased with the increase of LC3 binder content under the same spiked concentration (i.e., 192.82 mg/L for 4% LC3 vs. 14.57 mg/L for 10% LC3 in Zn1.5). In contrast, the leached Zn increased with the increase of spiked concentration under the same LC3 binder content (i.e., 4.83 mg/L for Zn0.5 vs. 56.87 mg/L for Zn1.5 in 8% LC3). Meanwhile, the increasing LC3 content enhances the leachate pH value from 4.85 to 7.02 due to the formation of portlandite (CH), which is one of the hydration products of cement (Buj et al., 2010).

The comparable results of TCLP after treating with LC3 and OPC binders are presented in Fig. 5b. Interestingly, the concentration of leachate Zn of OPC is lower than that of LC3 at Zn0.5, whereas is higher than that of LC3 at Zn1.5 at both the binder contents of 6% and 8%. The solubility of heavy-metal ions has previously been shown to be largely dependent on pH (Halim et al., 2003; de Andrade Lima and Bernardez, 2013). Meanwhile, the pH of OPC extracted solutions ranged from 6.0–7.6 but from 5.1–6.3 for the LC3.

The variation of leachate Zn and pH with different contents of LC3 in the SPLP test are presented in Fig. 6a. It can be seen that the leachate pH increased from 5 to 11.6 with the level of binder content. The leaching results have a similar tendency with TCLP. It can be observed that the leaching Zn of treated soils is lower than the critical regulator limit (100 mg/L in (SEPA, 2007)) regardless of the initial Zn concentration and curing age. The SPLP test results of Zn-contaminated soils mixed with LC3 and OPC binders are presented in Fig. 6b. The pH of the OPC leaching solution ranges from 10.6 to 11.8.
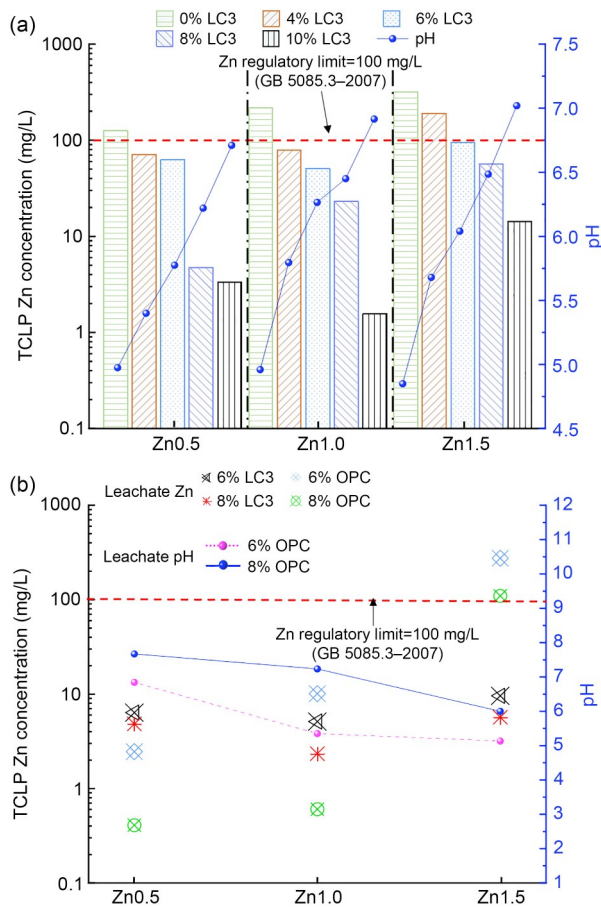
Fig. 5 Variation of TCLP leachate concentration and pH: (a) LC3 content; (b) LC3 vs. OPC (SEPA, 2007)

Fig. 6 Variation of SPLP leachate concentration and pH: (a) LC3 content; (b) LC3 vs. OPC (SEPA, 2007)

3.4 X-ray diffraction

The XRD results of 6% LC3 under various spiked Zn concentrations after curing for 28 d are presented in Fig. 7a. Previous research reports (Chen et al., 2019; Wang et al., 2019) have suggested that C–S–H and C–A–S–H are amorphous gels, depending on the Ca/Si ratio, Al/Si ratio, and the nanocrystalline structure. The substrate spacing of the C–S–H crystal appeared at 1.250, 0.307, 0.280, and 0.167 nm (Kapeluszna et al., 2017), and the substrate spacing of the C–A–S–H crystal is in the range of 0.900–1.600 nm (Geng et al., 2017). With the increase in the Ca/Si ratio, the crystallinity tended to decrease (Beaudoin and Odler, 2019). Therefore, in the LC3 ternary mixed system, the rich Si, Al, and the Ca/Si ratio meet the requirements for forming C–S–H and C–A–S–H crystals. As shown in Fig. 7a, the C–A–S–H crystals are not detected. In the S/S system, the formation of ettringite, C–S–H gel, and $CaAl_2Si_4O_{12}(H_2O)_2$ leads to the strength development (Liu et al., 2018).
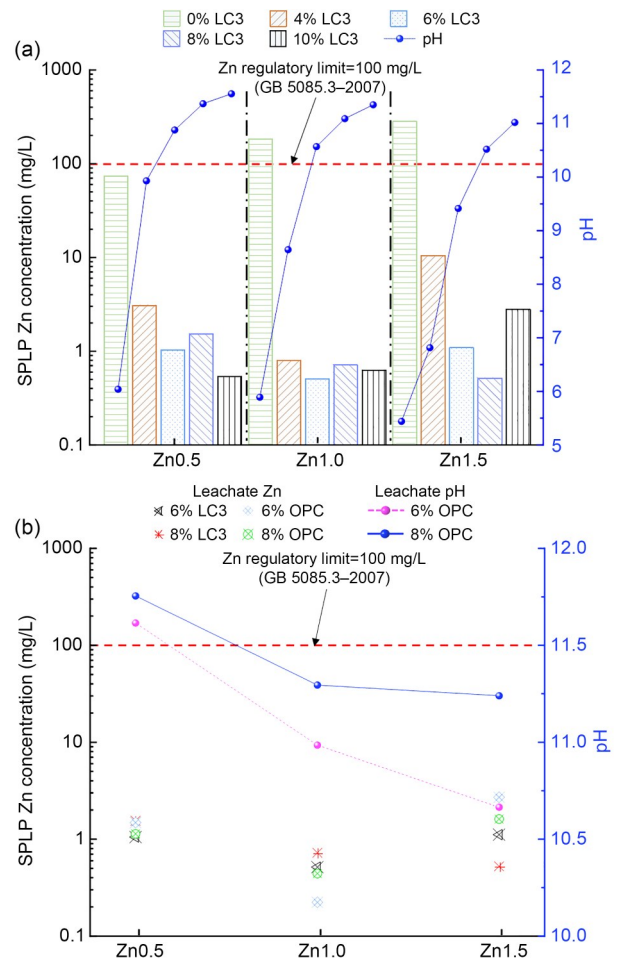
The XRD results of 6% LC3 and OPC S/S Zn1.5 Zn-contaminated soils cured for 28 d are presented in Fig. 7b. Additionally, the zinc silicate is identified in samples with a higher initial Zn concentration, while it cannot be detected in samples with a lower initial Zn concentration. In previous studies, it has been found that zinc silicate is not semi-permeable (Xue, 2018), and may cover the surface of LC3 particles. This alters the path of water molecules into the unhydrated particles and retards hydration products. Diffraction peaks such as quartz, calcite, and $Zn(OH)_2$ can be detected in the XRD pattern in Fig. 7b. Compared with the LC3 S/S sample, the XRD pattern of the OPC S/S sample does not identify minerals such as ettringite, calcium monocarbonate, and calcium aluminosilicate hydrate. Gu et al. (2020) also found ettringite and hydrated calcium aluminosilicate in LC3 S/S samples but they could not be detected in OPC S/S samples. In addition, Du et al. (2014) indicated that the presence of
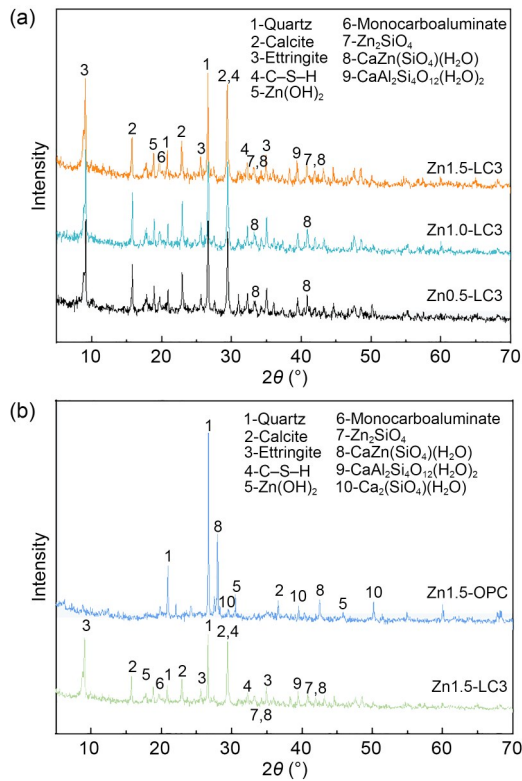
Fig. 7 XRD results: (a) LC3 S/S soils with different concentrations; (b) LC3 and OPC S/S soils

ettringite could not be detected at high Zn concentrations. However, ettringite can be detected in LC3 S/S samples with high Zn concentration in this study, which is probably because the addition of LS inhibits the conversion of aluminate ferrite trisubstituted (AFt) to aluminate ferrite monosubstituted (AFm).

3.5 Scanning electron microscope analysis

The SEM-EDS shows that needle-like and rod-like ettringite and hexagonal AFm phase appear on the surface of the Zn0.5-LC3 sample, and zinc hydroxide also covers the surface of soil aggregates in Fig. 8a. The existence of granular agglomerate zinc silicate is also observed on the surface of Zn1.5-LC3 sample, as shown in Fig. 8b. In Fig. 8c, on the surface of Zn1.5-OPC sample, the products such as ettringite and calcium AFm are not observed. The semi-transparent colloidal C–S–H and zinc hydroxide are observed. According to the EDS elemental map (Fig. 8d), the distribution of Zn observed on the Zn0.5-LC3 sample matrix is positively correlated with calcium, indicating the precipitation of calcium-zinc compounds. The distribution of carbon, aluminum, and oxygen is also positively

correlated, which again confirms the existence of the carbon aluminate AFm phase, consistent with the detection results of XRD. As shown in Fig. 8e, the distribution of silicon, aluminum, and oxygen is positively correlated, and the distribution of calcium is dense in the areas where silicon, aluminum, and oxygen appear, which proves the existence of C–S–H and C–A–S–H gels. The uniform distribution of Zn indicates that a large amount of Zn is adsorbed by gel products, such as C–S–H and C–A–S–H, produced by the hydration reaction.

4 Discussion

4.1 Solubility and precipitation pattern of Zn ions at various pH values

Generally, the solubility of Zn ions is highly pH-dependent, which is called amphoteric behavior (Kogbara et al., 2012). In this study, the chemical equilibrium model of Zn solubility at different pH values is evaluated through Visual MINTEQ 3.1, as shown in Fig. 9.

The observed behavior is similar for other series of experiments with different initial soluble Zn concentrations (i.e., 5000, 10000, and 15000 mg/L) as pH ranged from 2 to 14. Three regions of the precipitation/dissolution tendency can be divided in Fig. 9a. The solubility of Zn components reaches a maximum in the I-zone, which is assigned to acidic (pH=2−7) and severe alkaline conditions (pH=13−14). It can also be observed that the divalent cation (Zn^{2+}) and $Zn(OH)_4^{2-}$ are the major compounds when the pH is less than 7 and higher than 13, respectively. With an increase in pH above 7, the Zn^{2+} concentration gradually decreases to form a precipitate (i.e., $Zn(OH)_2$), as shown in II-zone. As the pH reaches 9.5–10.5, most of the soluble Zn^{2+} changes to the precipitated form (III-zone in Fig. 9a). When the pH is above 10.5, the $Zn(OH)_2$ precipitate begins to dissolve and form the soluble forms of $Zn(OH)_3^-$ and $Zn(OH)_4^{2-}$. The concentration of $Zn(OH)_3^-$ reaches its peak at pH=12. It was noted that the $Zn(OH)_2$ precipitate and the soluble $Zn(OH)_3^-$ and $Zn(OH)_4^{2-}$ are unstable in the II-zone. It can be concluded that the lower pH ranging from 7–10 causes higher precipitation as well as lower leaching Zn concentration. As shown in Fig. 5b, the concentration of leaching Zn in 8% OPC is lower than 8% LC3 and
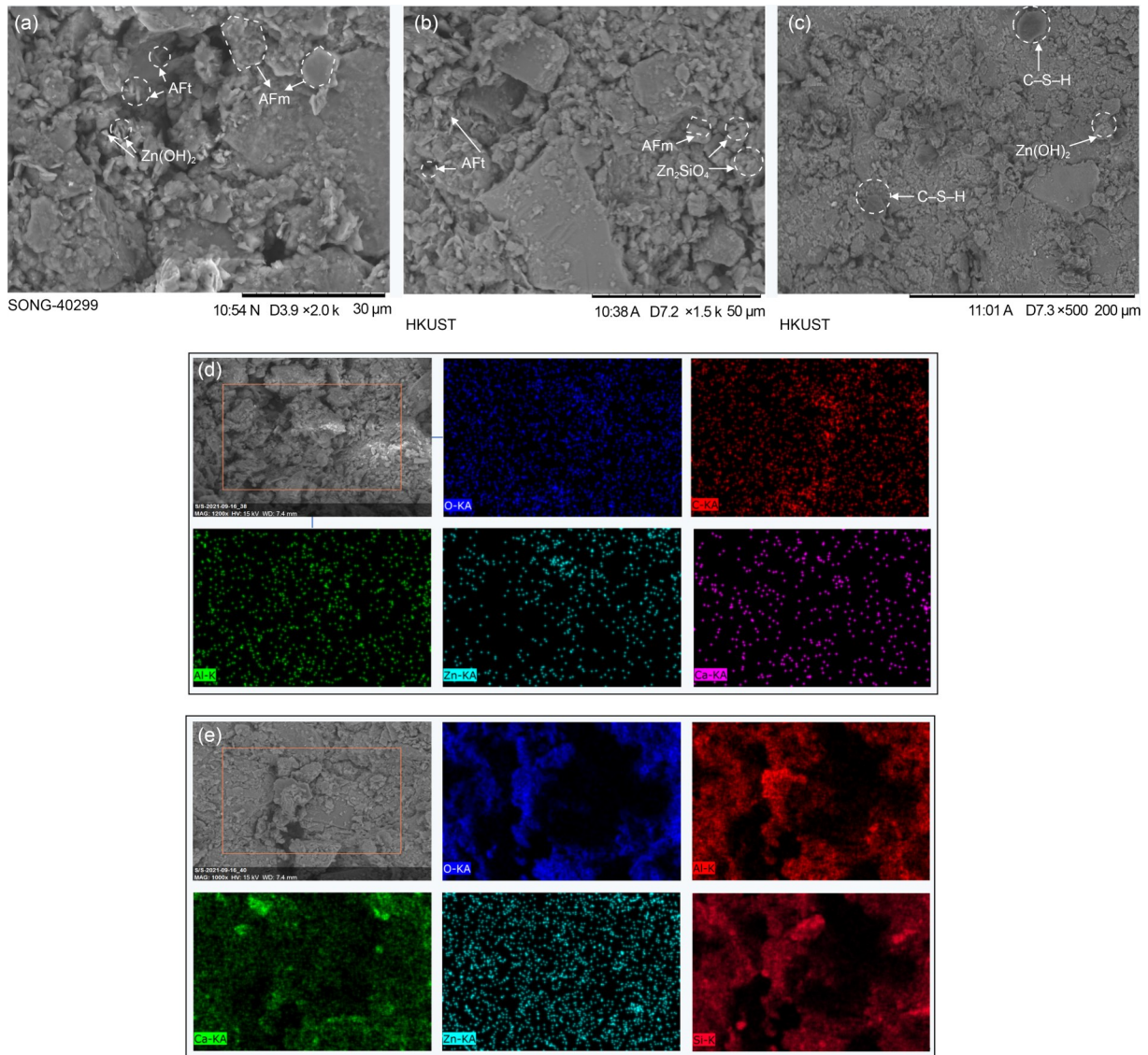
Fig. 8 SEM image with elemental mapping of 28-d cured soils: (a) Zn0.5-LC3; (b) Zn1.5-LC3; (c) Zn1.5-OPC; (d) element mapping of Zn0.5-LC3; (e) element mapping of Zn1.5-LC3

6% LC3 at the initial Zn1.0. The pH value of 7.24 in 8% OPC is higher than 6.45 for 8% LC3 and 6.26 for 6% LC3, indicating the free Zn is converted into more Zn precipitation in 8% OPC (Fig. 9). Since the pH of the LC3 leachate in the TCLP test is between 4.85 and 7.02, which is in I-zone in Fig. 9, Zn precipitation is not significantly affected by pH. Therefore, the focus here is on the phenomenon that occurs in the SPLP test. With an increase in LC3 content from 4% to 10%, the pH increases, while the Zn precipitation also changes with pH (Figs. 6 and 9). While LC3 content increases from 6% to 10%, Zn leaching concentration does not change significantly in SPLP tests

(Fig. 6). This phenomenon is attributed to the Zn0.5 composites being in dynamic equilibrium when the pH values of 6% LC3 and 10% LC3 range from 10.88 to 11.37. With this study's increasing initial Zn from Zn0.5 to Zn1.5 the corresponding leachate Zn increased from 63.63 to 95.92 mg/L (Fig. 5) under the 6% LC3, which indicates that the LC3 is efficient in stabilizing higher-level Zn contamination in soils.

4.2 Engineering properties of Zn-contaminated soils treated by LC3

Figs. 3 and 4 demonstrate that the UCS and k of the treated soils increase and decrease continuously
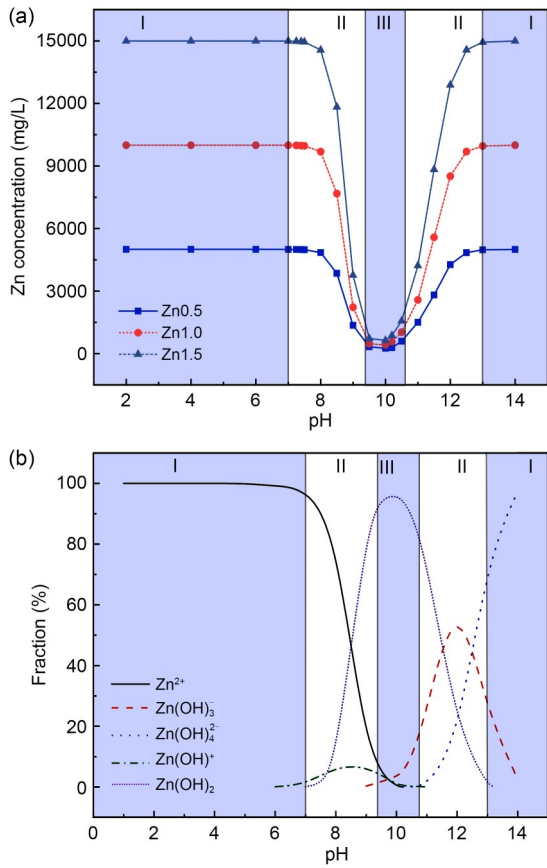
Fig. 9 Effect of pH on: (a) solubility; (b) precipitation pattern

after the addition of LC3 to Zn-contaminated soils. This is attributed to the formation of hydration products, i.e., C–S–H and ettringite (Fig. 7), which fill the pores between the soil particles (Figs. 10a and 10f). Additionally, C–S–H and C–A–S–H gels aggregate soil particles into larger clusters (Fig. 10e), reducing k. In response to increasing Zn concentration, the compressive strength of the soil decreased and its permeability increased. With increasing Zn concentration from Zn0.5 to Zn1.5, the mechanical UCS decreased in a significant way, from approximately 2.11 to 1.78 MPa at 28 d. It also increased k, from about 2.71×10^{-8} to 3.78×10^{-8} cm/s due to the larger pore structure. In addition, it covered the surface of the LC3 particles with zinc hydroxide and zinc silicate (Figs. 7 and 8), which will also reduce the nucleation sites for hydration gel products, i.e., C–S–H and C–A–S–H. The LC3 samples exhibited superior compression strength and lower k compared with the OPC samples, which may be attributed to the well-filled pore effect because of the fineness of LS and calcinated kaolin powder (Dixit et al., 2021; Drissi et al., 2021; Yu et al., 2021). Furthermore, the calcinated kaolin provided sufficient Al source to form flocculant $CaAl_2Si_4O_{12}(H_2O)_2$, which bonded the ettringite together and reduced the macropores (Zhang et al., 2020). Moreover, a regression analysis was
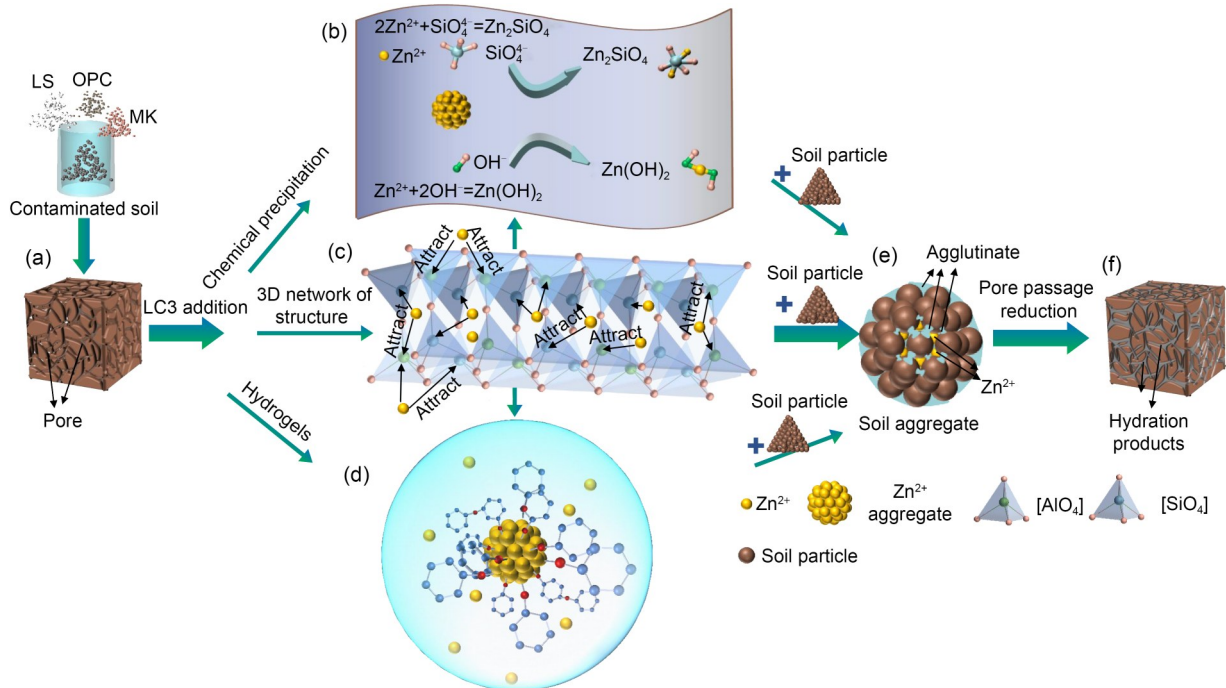

Fig. 10 S/S mechanism diagram: (a) contaminated soils; (b) chemical precipitation;(c) 3D network structure of charge balance in Si–Al system; (d) hydrogels; (e) soil aggregate; (f) treated

conducted to identify the correlation between hydraulic conductivity and strength. It can be seen that the hydraulic conductivity tends to decrease as the strength increases (Fig. 11).
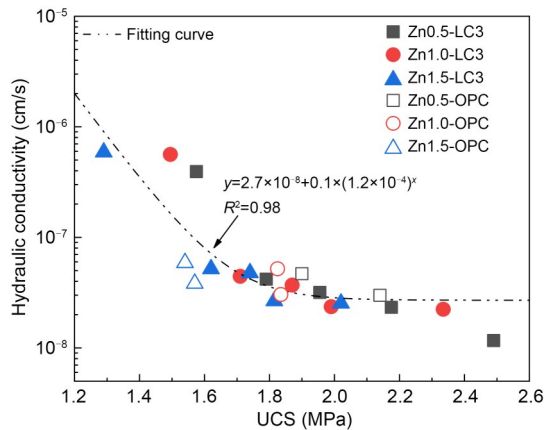

Fig. 11 Correlation between hydraulic conductivity and UCS based on Zn concentration and binders

4.3 Immobilization mechanism of Zn-contaminated soils treated by LC3

Fig. 10 summarizes the S/S mechanism of Zn-contaminated soils, including macro-encapsulation, micro-encapsulation, chemical stability, and ion exchange, as well as surface absorption and adsorption in crystal lattices. Figs. 5 and 6 show that the criterion of Zn leaching concentration stipulated by China is only exceeded in TCLP leaching tests when the initial Zn concentration is 15000 mg/kg and the content of LC3 is 4%. As compared to OPC, the lower leaching concentration of Zn with LC3 treatment is primarily attributed to:

1. The existence of chemical precipitation, i.e., $Zn(OH)_2$ and Zn_2SiO_4 (Figs. 7 and 10b), could be found in both OPC and LC3 treated contaminated soils, which has also been reported by previous studies (Qian et al., 2003; Reddy et al., 2020), whereas the ettringite merely occurred in the Zn-contaminated soils treated by a binder of LC3. During the S/S process, the ettringite captured free Zn into the lattice (Albino et al., 1996), leading to a lower leaching concentration, as shown in Fig. 5.

2. The pozzolanic reaction produces hydrated products, i.e., C–A–S–H and C–S–H gels, which have a high ion exchange energy and special surface area (Garcia-Lodeiro et al., 2011; Huang et al., 2016; Zhang

et al., 2021). These are beneficial for encapsulating the free Zn ions (Fig. 10d). Additionally, the C–A–S–H and C–S–H gels crystallize with curing ages, forming a stiff matrix and binding the soil particles by infilling the inter-aggregate pore, thus isolating the free Zn from the external environment.

3. Furthermore, the free Zn ions can be efficiently solidified in the tetrahedral structure of $[SiO_4]$ and $[AlO_4]$ (Peng et al., 2019; Wang et al., 2020), which is a typic crystalline structure of the rich Si and Al in LC3 (Fig. 10c). The Al and Si in the 3D network structure of $[SiO_4]$ and $[AlO_4]$ tetrahedrons can be substituted by Zn (Peng et al., 2019). According to Zhang et al. (2020), divalent ions have a better equilibrium valence state than monovalent ions in the S/S system. Therefore, the free Zn ions replace Si or Al in $[SiO_4]$ and $[AlO_4]$ tetrahedrons to form the stable mineral $CaZn(SiO_4)(H_2O)$ and Zn_2SiO_4 (Figs. 7, 10b, and 10c), which is more effective than adsorption and physical encapsulation (Peng et al., 2019).

5 Conclusions

This research ascertained the feasibility of developing an effective LC3 binder to replace the OPC in treating Zn-contaminated soils and investigated its engineering properties and immobilization potential. The UCS and k of the LC3 treated Zn-contaminated soils increase and decrease with the increase of curing time and binder content, respectively. A negative correlation between UCS and k of LC3 and OPC-solidified contaminated soils is observed as the binder content and Zn concentration ranged from 0% to 10% and 0 to Zn1.5, respectively. k can be inferred from the UCS of a certain Zn concentration according to the empirical formula. With increasing Zn concentration from Zn0.5 to Zn1.5, the UCS significantly dropped from 2.11 to 1.78 MPa at 28 d, and the k increased from 2.71×10^{-8} to 3.78×10^{-8} cm/s. For the leachability, the Zn leaching concentration stipulated by China is only exceeded in TCLP leaching tests when the initial Zn concentration is 15000 mg/kg and the content of LC3 is 4%. The model simulation of solubility and precipitation pattern reasonably matched the Zn extraction and pH value from the TCLP and SPLP tests, illustrating the capability of the proposed model for providing a prior and quantitative estimation of

LC3-stabilized contaminated soils. The formations of hydration products, i.e., $Zn(OH)_2$, Zn_2SiO_4, C–S–H, C–A–S–H gel, ettringite, and $CaZn(SiO_4)(H_2O)$, which are the primary mechanisms for the immobilization of Zn in the LC3 treated contaminated soils are demonstrated. Furthermore, previous researchers observed that C–S–H and C–A–S–H gels have still been able to treat Zn, Pb, and Cd, which demonstrates that the LC3 binder also has long-term durability (Pandey et al., 2012). Further research should consider scenario-contaminated soils as compared to an artificially contaminated one. Further, the X-ray photoelectron spectroscopy (XPS) test and oxidation reduction potential (ORP) value should also be conducted in future investigations.

Acknowledgments

Author contributions

Haoliang WU processed the corresponding data and organized the manuscript. Heng SONG wrote the first draft of the manuscript. Xinpo SUN, Yuzhang BI, Shenjing FU, and Ning YANG helped to conduct experiments. Haoliang WU designed the research and revised and edited the final version.

Conflict of interest

Haoliang WU, Heng SONG, Xinpo SUN, Yuzhang BI, Shenjing FU, and Ning YANG declare that they have no conflict of interest.

References

Albino V, Cioffi R, Marroccoli M, et al., 1996. Potential application of ettringite generating systems for hazardous waste stabilization. *Journal of Hazardous Materials*, 51(1-3): 241-252.
https://doi.org/10.1016/S0304-3894(96)01828-6

Avet F, Snellings R, Diaz AA, et al., 2016. Development of a new rapid, relevant and reliable (R^3) test method to evaluate the pozzolanic reactivity of calcined kaolinitic clays. *Cement and Concrete Research*, 85:1-11.
https://doi.org/10.1016/j.cemconres.2016.02.015

Bakera AT, Alexander MG, 2019. Use of metakaolin as supplementary cementitious material in concrete, with focus on durability properties. *RILEM Technical Letters*, 4:89-102.
https://doi.org/10.21809/rilemtechlett.2019.94

Beaudoin J, Odler I, 2019. Hydration, setting and hardening of Portland cement. *In*: Hewlett PC, Liska M (Eds.), Lea's Chemistry of Cement and Concrete, 5th Edition.

Butterworth-Heinemann, Cambridge, UK, p.157-250.
https://doi.org/10.1016/B978-0-08-100773-0.00005-8

Bucher R, Diederich P, Escadeillas G, et al., 2017. Service life of metakaolin-based concrete exposed to carbonation: comparison with blended cement containing fly ash, blast furnace slag and limestone filler. *Cement and Concrete Research*, 99:18-29.
https://doi.org/10.1016/j.cemconres.2017.04.013

Buj I, Torras J, Rovira M, et al., 2010. Leaching behaviour of magnesium phosphate cements containing high quantities of heavy metals. *Journal of Hazardous Materials*, 175(1-3):789-794.
https://doi.org/10.1016/j.jhazmat.2009.10.077

Capasso I, Lirer S, Flora A, et al., 2019. Reuse of mining waste as aggregates in fly ash-based geopolymers. *Journal of Cleaner Production*, 220:65-73.
https://doi.org/10.1016/j.jclepro.2019.02.164

Chen J, Chen JZ, Tan MZ, et al., 2002. Soil degradation: a global problem endangering sustainable development. *Journal of Geographical Sciences*, 12(2):243-252.
https://doi.org/10.1007/BF02837480

Chen L, Wang L, Cho DW, et al., 2019. Sustainable stabilization/solidification of municipal solid waste incinerator fly ash by incorporation of green materials. *Journal of Cleaner Production*, 222:335-343.
https://doi.org/10.1016/j.jclepro.2019.03.057

Choi YC, Park B, 2020. Effects of high-temperature exposure on fractal dimension of fly-ash-based geopolymer composites. *Journal of Materials Research and Technology*, 9(4):7655-7668.
https://doi.org/10.1016/j.jmrt.2020.05.034

Cuisinier O, Le Borgne T, Deneele D, et al., 2011. Quantification of the effects of nitrates, phosphates and chlorides on soil stabilization with lime and cement. *Engineering Geology*, 117(3-4):229-235.
https://doi.org/10.1016/j.enggeo.2010.11.002

de Andrade Lima LRP, Bernardez LA, 2013. Evaluation of the chemical stability of a landfilled primary lead smelting slag. *Environmental Earth Sciences*, 68(4):1033-1040.
https://doi.org/10.1007/s12665-012-1805-x

Deng L, Shi Z, 2015. Synthesis and characterization of a novel Mg–Al hydrotalcite-loaded kaolin clay and its adsorption properties for phosphate in aqueous solution. *Journal of Alloys and Compounds*, 637:188-196.
https://doi.org/10.1016/j.jallcom.2015.03.022

Dixit A, Du HJ, Pang SD, 2021. Performance of mortar incorporating calcined marine clays with varying kaolinite content. *Journal of Cleaner Production*, 282:124513.
https://doi.org/10.1016/j.jclepro.2020.124513

Drissi S, Shi CJ, Li N, et al., 2021. Relationship between the composition and hydration-microstructure-mechanical properties of cement-metakaolin-limestone ternary system. *Construction and Building Materials*, 302:124175.
https://doi.org/10.1016/j.conbuildmat.2021.124175

Du YJ, Jiang NJ, Liu SY, et al., 2014. Engineering properties and microstructural characteristics of cement-stabilized zinc-contaminated kaolin. *Canadian Geotechnical Journal*,

51(3):289-302.
https://doi.org/10.1139/cgj-2013-0177

Elbltagy HM, Elbasiouny H, Almuhamady A, et al., 2021. Low cost and eco-friendly removal of toxic heavy metal from industrial wastewater. *Egyptian Journal of Soil Science*, 61(2):219-229.
https://doi.org/10.21608/ejss.2021.75492.1444

Garcia-Lodeiro I, Palomo A, Fernández-Jiménez A, et al., 2011. Compatibility studies between N-A-S-H and C-A-S-H gels. Study in the ternary diagram Na_2O–CaO–Al_2O_3–SiO_2–H_2O. *Cement and Concrete Research*, 41(9):923-931.
https://doi.org/10.1016/j.cemconres.2011.05.006

Geng GQ, Myers RJ, Li JQ, et al., 2017. Aluminum-induced dreierketten chain cross-links increase the mechanical properties of nanocrystalline calcium aluminosilicate hydrate. *Scientific Reports*, 7:44032.
https://doi.org/10.1038/srep44032

Gu YC, Li JL, Peng JK, et al., 2020. Immobilization of hazardous ferronickel slag treated using ternary limestone calcined clay cement. *Construction and Building Materials*, 250:118837.
https://doi.org/10.1016/j.conbuildmat.2020.118837

Halim CE, Amal R, Beydoun D, et al., 2003. Evaluating the applicability of a modified toxicity characteristic leaching procedure (TCLP) for the classification of cementitious wastes containing lead and cadmium. *Journal of Hazardous Materials*, 103(1-2):125-140.
https://doi.org/10.1016/S0304-3894(03)00245-0

Han RR, Zhou BH, Huang YY, et al., 2020. Bibliometric overview of research trends on heavy metal health risks and impacts in 1989–2018. *Journal of Cleaner Production*, 276:123249.
https://doi.org/10.1016/j.jclepro.2020.123249

Hosan A, Shaikh FUA, 2021. Compressive strength development and durability properties of high volume slag and slag-fly ash blended concretes containing nano-$CaCO_3$. *Journal of Materials Research and Technology*, 10:1310-1322.
https://doi.org/10.1016/j.jmrt.2021.01.001

Huang X, Huang T, Li S, et al., 2016. Immobilization of chromite ore processing residue with alkali-activated blast furnace slag-based geopolymer. *Ceramics International*, 42(8):9538-9549.
https://doi.org/10.1016/j.ceramint.2016.03.033

Kapeluszna E, Kotwica Ł, Różycka A, et al., 2017. Incorporation of Al in C-A-S-H gels with various Ca/Si and Al/Si ratio: microstructural and structural characteristics with DTA/TG, XRD, FTIR and TEM analysis. *Construction and Building Materials*, 155:643-653.
https://doi.org/10.1016/j.conbuildmat.2017.08.091

Khalid S, Shahid M, Niazi NK, et al., 2017. A comparison of technologies for remediation of heavy metal contaminated soils. *Journal of Geochemical Exploration*, 182:247-268.
https://doi.org/10.1016/j.gexplo.2016.11.021

Kogbara RB, Al-Tabbaa A, Yi YL, et al., 2012. pH-dependent leaching behaviour and other performance properties of cement-treated mixed contaminated soil. *Journal of Environmental Sciences*, 24(9):1630-1638.
https://doi.org/10.1016/S1001-0742(11)60991-1

Kua TA, Arulrajah A, Horpibulsuk S, et al., 2016. Strength assessment of spent coffee grounds-geopolymer cement utilizing slag and fly ash precursors. *Construction and Building Materials*, 115:565-575.
https://doi.org/10.1016/j.conbuildmat.2016.04.021

Liu XM, Zhao XB, Yin HF, et al., 2018. Intermediate-calcium based cementitious materials prepared by MSWI fly ash and other solid wastes: hydration characteristics and heavy metals solidification behavior. *Journal of Hazardous Materials*, 349:262-271.
https://doi.org/10.1016/j.jhazmat.2017.12.072

MEP (Ministry of Environmental Protection of the People's Republic of China), 2014. China Soil Pollution Survey Communique. MEP, Beijing, China (in Chinese).

Moghal AAB, Ashfaq M, Al-Shamrani MA, et al., 2020. Effect of heavy metal contamination on the compressibility and strength characteristics of chemically modified semiarid soils. *Journal of Hazardous, Toxic, and Radioactive Waste*, 24(4):04020029.
https://doi.org/10.1061/(ASCE)HZ.2153-5515.0000527

MWR (Ministry of Water Resources of the People's Republic of China), 2019. Standard for Geotechnical Testing Method, GB/T 50123–2019. National Standards of the People's Republic of China (in Chinese).

Pandey B, Kinrade SD, Catalan LJJ, 2012. Effects of carbonation on the leachability and compressive strength of cement-solidified and geopolymer-solidified synthetic metal wastes. *Journal of Environmental Management*, 101:59-67.
https://doi.org/10.1016/j.jenvman.2012.01.029

Pantazopoulou E, Ntinoudi E, Zouboulis AI, et al., 2020. Heavy metal stabilization of industrial solid wastes using low-grade magnesia, Portland and magnesia cements. *Journal of Material Cycles and Waste Management*, 22(4):975-985.
https://doi.org/10.1007/s10163-020-00985-9

Paria S, Yuet PK, 2006. Solidification–stabilization of organic and inorganic contaminants using Portland cement: a literature review. *Environmental Reviews*, 14(4):217-255.
https://doi.org/10.1139/a06-004

Parus A, Framski G, 2018. Impact of *O*-alkyl-pyridineamidoximes on the soil environment. *Science of the Total Environment*, 643:1278-1284.
https://doi.org/10.1016/j.scitotenv.2018.06.266

Parus A, Idziak M, Jacewicz P, et al., 2021. Assessment of environmental risk caused by the presence of antibiotics. *Environmental Nanotechnology, Monitoring & Management*, 16:100533.
https://doi.org/10.1016/j.enmm.2021.100533

Peng DD, Wang YG, Liu XM, et al., 2019. Preparation, characterization, and application of an eco-friendly sand-fixing material largely utilizing coal-based solid waste. *Journal of Hazardous Materials*, 373:294-302.
https://doi.org/10.1016/j.jhazmat.2019.03.092

Qian GR, Sun DD, Tay JH, 2003. Immobilization of mercury and zinc in an alkali-activated slag matrix. *Journal of Hazardous Materials*, 101(1):65-77.
https://doi.org/10.1016/S0304-3894(03)00143-2

Reddy VA, Solanki CH, Kumar S, et al., 2019. New ternary blend limestone calcined clay cement for solidification/ stabilization of zinc contaminated soil. *Chemosphere*, 235:308-315.
https://doi.org/10.1016/j.chemosphere.2019.06.051

Reddy VA, Solanki CH, Kumar S, et al., 2020. Stabilization/ solidification of zinc- and lead-contaminated soil using limestone calcined clay cement (LC^3): an environmentally friendly alternative. *Sustainability*, 12(9):3725.
https://doi.org/10.3390/su12093725

Reddy VA, Solanki CH, Kumar S, et al., 2022. Comparison of limestone calcined clay cement and ordinary Portland cement for stabilization/solidification of Pb-Zn smelter residue. *Environmental Science and Pollution Research*, 29(8):11393-11404.
https://doi.org/10.1007/s11356-021-16421-w

Scrivener KL, 2014. Options for the future of cement. *The Indian Concrete Journal*, 88(7):11-21.

Senneca O, Cortese L, di Martino R, et al., 2020. Mechanisms affecting the delayed efficiency of cement based stabilization/ solidification processes. *Journal of Cleaner Production*, 261:121230.
https://doi.org/10.1016/j.jclepro.2020.121230

Snehal K, Das B, 2022. Pozzolanic reactivity and drying shrinkage characteristics of optimized blended cementitious composites comprising of Nano-Silica particles. *Construction and Building Materials*, 316:125796.
https://doi.org/10.1016/j.conbuildmat.2021.125796

SEPA (State Environmental Protection Administration), 2007. Identification Standards for Hazardous Wastes–Identification for Extraction Toxicity, GB 5085.3–2007. National Standards of the People's Republic of China (in Chinese).

Tang J, Wei SF, Li WF, et al., 2019. Synergistic effect of metakaolin and limestone on the hydration properties of Portland cement. *Construction and Building Materials*, 223:177-184.
https://doi.org/10.1016/j.conbuildmat.2019.06.059

USEPA (United States Environmental Protection Agency), 1992. SW-846 Test Method 1311: Toxicity Characteristic Leaching Procedure. USEPA, USA.

USEPA (United States Environmental Protection Agency), 1994. SW-846 Test Method 1312: Synthetic Precipitation Leaching Procedure. USEPA, USA.

Wang H, Hou PK, Li QF, et al., 2021. Synergistic effects of supplementary cementitious materials in limestone and calcined clay-replaced slag cement. *Construction and Building Materials*, 282:122648.
https://doi.org/10.1016/j.conbuildmat.2021.122648

Wang L, Chen L, Tsang DCW, et al., 2018. Green remediation of contaminated sediment by stabilization/solidification with industrial by-products and CO_2 utilization. *Science of the Total Environment*, 631-632:1321-1327.
https://doi.org/10.1016/j.scitotenv.2018.03.103

Wang L, Cho DW, Tsang DCW, et al., 2019. Green remediation of As and Pb contaminated soil using cement-free clay-based stabilization/solidification. *Environment International*, 126:336-345.
https://doi.org/10.1016/j.envint.2019.02.057

Wang L, Geddes DA, Walkley B, et al., 2020. The role of zinc in metakaolin-based geopolymers. *Cement and Concrete Research*, 136:106194.
https://doi.org/10.1016/j.cemconres.2020.106194

Wu HL, Jin F, Bo YL, et al., 2018. Leaching and microstructural properties of lead contaminated kaolin stabilized by GGBS-MgO in semi-dynamic leaching tests. *Construction and Building Materials*, 172:626-634.
https://doi.org/10.1016/j.conbuildmat.2018.03.164

Xue ST, 2018. Study on the Effect and Mechanism of Zinc Compounds on the Properties of Cement-Based Materials. MS Thesis, Zhejiang University of Technology, Hangzhou, China (in Chinese).

Yadav AL, Sairam V, Muruganandam L, et al., 2020. An overview of the influences of mechanical and chemical processing on sugarcane bagasse ash characterisation as a supplementary cementitious material. *Journal of Cleaner Production*, 245:118854.
https://doi.org/10.1016/j.jclepro.2019.118854

Yu J, Wu HL, Mishra DK, et al., 2021. Compressive strength and environmental impact of sustainable blended cement with high-dosage limestone and calcined clay (LC2). *Journal of Cleaner Production*, 278:123616.
https://doi.org/10.1016/j.jclepro.2020.123616

Zhang YL, Liu XM, Xu YT, et al., 2020. Preparation of road base material by utilizing electrolytic manganese residue based on Si-Al structure: mechanical properties and Mn^{2+} stabilization/solidification characterization. *Journal of Hazardous Materials*, 390:122188.
https://doi.org/10.1016/j.jhazmat.2020.122188

Zhang YY, Wang L, Chen L, et al., 2021. Treatment of municipal solid waste incineration fly ash: state-of-the-art technologies and future perspectives. *Journal of Hazardous Materials*, 411:125132.
https://doi.org/10.1016/j.jhazmat.2021.125132